Raman and infrared studies of the CN^- stretching-mode anharmonicity and its relation to phase transitions in pure alkali cyanides

Dominique Durand
Centre Lorrain d'Optique et Electronique des Solides (CLOES), Ecole Superieure d'Electricité, Université de Metz, Technopôle de Metz, 57078 Metz CEDEX 03, France

Luiz Carlos Scavarda do Carmo
Departmento de Física, Pontifícia Universidade Católica do Rio de Janeiro, 22 452 Rio de Janeiro, Rio de Janeiro, Brazil

Fritz Lüty
Department of Physics, University of Utah, Salt Lake City, Utah 84112
(Received 12 November 1987; revised manuscript received 22 August 1988)

A comprehensive ir and Raman study of the fundamental and overtone stretching modes of CN^- molecules in pure alkali cyanides has been performed. Peak position, half-width, and strength of these modes have been measured—as far as is accessible with both techniques—between 4 and 300 K through the phases of different order in pure NaCN, KCN, RbCN, and CsCN. From the main data, we first derive a general anharmonic-oscillator model for a single CN^- in different hosts, determining anharmonicity constants, dissociation energy, polarizability derivatives, etc., and comparing them to calculated values and models. More detailed changes observed in frequency and width and strength of the transitions under temperature variation can be related to elastic deformations and changes in CN^- rotational freedom and interaction effects in the different phases. In particular, a sideband with characteristic temperature dependence of splitting and strength observed in KCN and NaCN reveals the gradual buildup of internal electric field and antiferroelectric order by its pronounced effect on the CN^- oscillator. The absence of this effect in RbCN and CsCN confirms the absence of electric order in these materials.

I. INTRODUCTION

The alkali cyanides—materials with both ionic and molecular crystal features—display order-disorder behavior characteristic for a large group of materials of the type $M^+(XY)^-$. At high temperatures, rapid reorientation processes of the linear $(XY)^-$ [$=CN^-$] molecule average out all molecular anisotropies, so that a *pseudocubic structure* and quasi–alkali-halide behavior results (KCN, NaCN, and RbCN in the sodium chloride structure; CsCN in the cesium chloride structure). Under cooling to a first critical temperature T_{C1}, all four materials undergo a *first-order phase transition* (with sharp specific heat anomalies[1]), in which the "elastic dipoles"—the elliptically shaped CN^- molecules—align in an ordered way. In NaCN and KCN, the molecular axes align all parallel—"*ferroelastically*"—close to the ⟨110⟩ directions of the original cubic crystal, producing a strong shearing (T_{2g}) and tetragonal contraction (E_g) of the cubic cell and resulting in the formation of an *orthorhombic structure.*[2] For RbCN the earlier assumed parallel ordered phase[3,4] has been corrected by a recent neutron diffraction study;[5] this showed a monoclinic lattice, consisting of two groups of (equal number) CN^- molecules, aligned in different (nearly perpendicular) orientations—i.e., arranged in an "*antiferroelastic*" order. Contrary to this, the early determined rhombohedral structure of CsCN with parallel order of all CN^- molecules[3] was confirmed by recent neutron and x-ray work.[6]

In all four cases the strong elastic distortions connected with the CN^- ordering at T_{C1} lead to the formation of a *domain structure*[7,8] and strong light scattering due to the different orientations of the optical axes of the birefringent domains.[9] Below T_{C1}, the CN^- molecules are not yet ordered in terms of their head and tail, and—as dielectric measurements show—the CN^- electric dipoles are still able to perform reorientation motion.[10,11] In KCN and NaCN, this remaining electric disorder and degree of freedom is gradually removed under cooling below a second critical temperature T_{C2}, producing a broad specific heat anomaly[1] and gradual decrease of the dipolar polarizability.[10] According to neutron data,[12,13] the final resulting order at low temperatures consists for these two materials of planes of parallel electric dipoles with alternating signs among neighboring planes along the b axis. For the RbCN and CsCN systems, no T_{C2} specific heat anomaly has been observed.[14] Dielectric measurements show for RbCN paraelectric Curie law behavior[11] down to 33 K and low reorientation rates ($\tau^{-1} \sim 10^{-2}$ sec^{-1}), leading under further cooling around 30 K to freezing into an orientationally disordered dipolar glass state.[15]

The linear diatomic structure of the CN^- molecules

(replacing the spherical halide molecule of alkali halides) introduces two new motional degrees of freedom, *rotational and stretching modes* of the molecule. The first ones lie in the frequency range (0–250 cm^{-1}) of lattice phonons, so that strong rotational-translational coupling occurs.[16] The resulting coupled modes have been intensely investigated, in direct excitation by Raman[17–19] and far-ir (Ref. 13) spectroscopy, or as combination spectra[20] of the stretch band. The pure mode at ~ 2100 cm^{-1}, on the other hand, lies far outside the phonon frequency range, so that coupling to translational modes can be neglected.[21] The stretching mode has been observed in many previous ir and Raman studies,[17–19,22] but no systematic and comprehensive study through the various alkali cyanides and their different phases has been performed. This is what we attempt in this work.

An obvious approach to the CN^- stretching properties is from the well studied case of *dilute substitutional* CN^- *defects, isolated in alkali halides.*[23,24] Figure 1 summarizes the stretching frequencies CN^- defects observed (at 90 K) in twelve alkali halides.[24] The frequencies clearly vary systematically with cation and anion size (maximum relative variation $\Delta\nu/\nu < 2.5\%$), shifting to higher energies with increasing lattice parameters. Measured frequency shifts under hydrostatic pressure[24] agree closely with this variation. Model calculations showed that the small effects of the crystal environment can be well accounted for by a static potential of essentially Born Mayer type, in which frequency shifts are dominated by repulsive forces, which shorten the CN^- bond lengths through the negative anharmonicity term.[24] This behavior is preserved when going from isolated CN^- defects to the CN^- sublattice of pure alkali cyanides. The lattice parameter of the latter (in the cubic phase) is very close to the ones of alkali bromides, and the CN^- stretching frequencies in the two types of systems coincide indeed very closely, as Fig. 1 shows.

A similar empirical connection between the isolated and sublattice CN^- case can be made for the *integrated strength of the stretching absorption.* Figure 2 shows in double logarithmic scale the integrated absorption of the first and second harmonic CN^- stretching as a function of CN^- concentration x, measured through the KCl_{1-x}:KCN_x and KBr_{1-x}:KCN_x mixtures. In both systems a linear scaling of the fundamental and overtone absorption with x is observed, showing that interaction effects among CN^- dipoles do not affect appreciably the measured quantities. Similar scaling of the integrated fundamental stretching response with CN^- concentration has been observed with Raman techniques.[25]

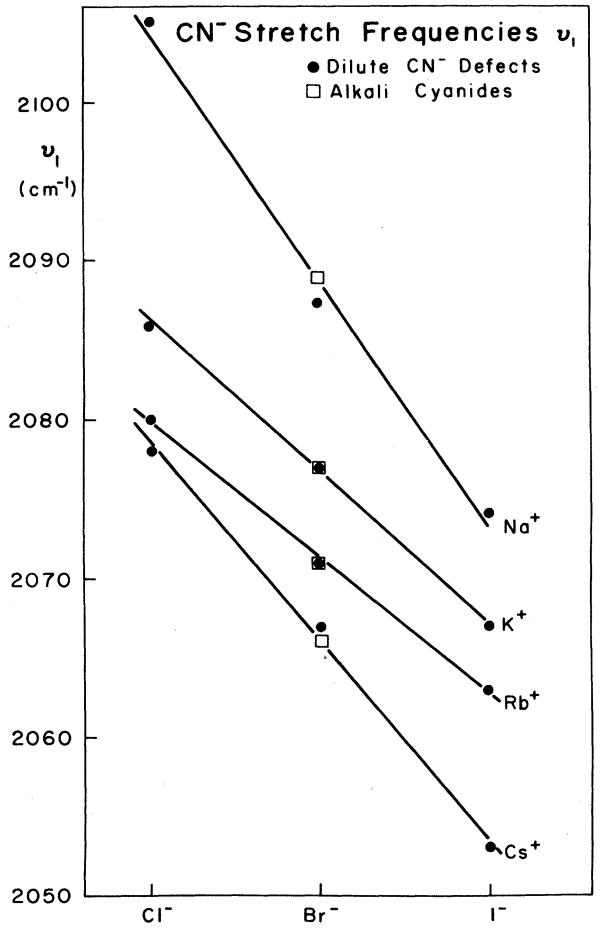

FIG. 1. CN^- stretching frequency ν_1, observed with ir absorption for dilute CN^- defects in 12 alkali halide hosts and for the four pure alkali cyanides. [Spectral positions, widths and shapes in all figures are represented in wave number (cm^{-1}) scales.]

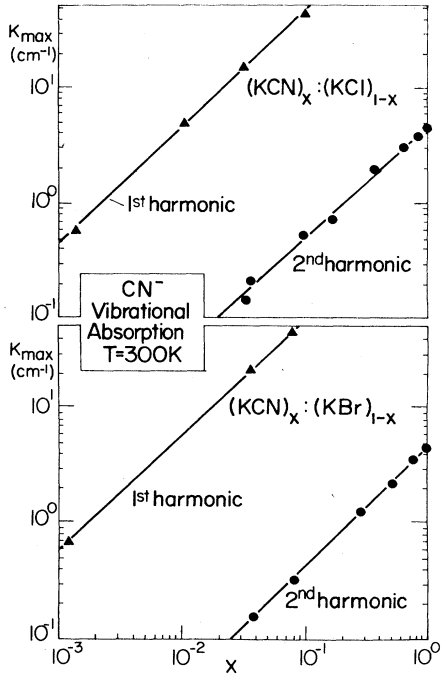

FIG. 2. Integrated first and second harmonic ir absorption (ν_1 and ν_2) of stretching CN^- bands in two mixed alkali-halide-alkali-cyanide systems, measured as a function of the mole ratio x of KCN.

Obviously, the stretching mode of the CN^- molecule must be regarded very much as an individual internal molecular property: it scales in strength with the number CN^- dipoles, preserves a rather constant anharmonicity (as seen by the constant overtone: fundamental ratio and by the constant shift of the overtone frequency from the double fundamental frequency), and is affected only slightly in its eigenfrequency by the lattice parameter of the environment. In spite of this "environmentally insensitive" character of the CN^- stretching mode, we will explore in this work, to what degree this mode can be used as an internal (infrared and Raman) probe for the study of the various phases and environmental changes occurring in the four pure alkali cyanides between 300 and 5 K. It is evident from the above discussion that the expected effects will be small and therefore require high accuracy of measurements.

II. EXPERIMENTAL RESULTS

The single crystals used in this work were pulled from the melt (under Ar atmosphere) from highly pure—mostly zone-refined—material in the Utah Crystal Laboratory. Raman measurements were performed with 4880-Å excitation from an Ar^+ laser, using a Spex double grating spectrometer with photon counting. Plasma emission lines from the Ar^+ laser were used for absolute wavelength calibration (accuracy $\sim\pm1$ cm^{-1}). The ir measurements were performed for the fundamental region with a Beckman 4250 and Perkin Elmer 180 spectrometer, for the overtone region with a Cary 14 instrument, with estimated accuracies of ±2, ±2, and ±1 cm^{-1}, respectively. The presentation of the data will be divided by the two employed techniques.

A. Raman results

Figure 3 gives a summary of part of the Raman measurements on the 1st harmonic (ν_1) stretching mode, recorded in the four materials at various temperatures. [These—and all subsequent—Raman spectra are unpolarized and represent essentially the A_{1g} scattering which constitutes by far (>95%) the largest part of the total Raman response.] As Fig. 3 shows, clearly detectable changes of peak position (ν) and bandwidth (H) occur in all four materials under temperature and phase variation. These changes in position (~first moment) and width (~second moment) of the bands is plotted as a function of temperature for the four materials in Figs. 4 and 5, respectively. [No attempt was made to detect with Raman scattering any possible variation of the integrated strength (~zeroth moment) of the bands, due to the high experimental uncertainty especially in the regime of crystal opacity below T_{C1}.] Figures 4 and 5 show that the known critical temperatures T_{C1} and T_{C2} in the four materials (indicated by arrows) show up by distinct changes of the values and/or slopes of the $\nu(T)$ and $H(T)$ curves. In all four materials the half-width H increases abruptly with cooling through T_{C1} into the ferroelastic phase. For

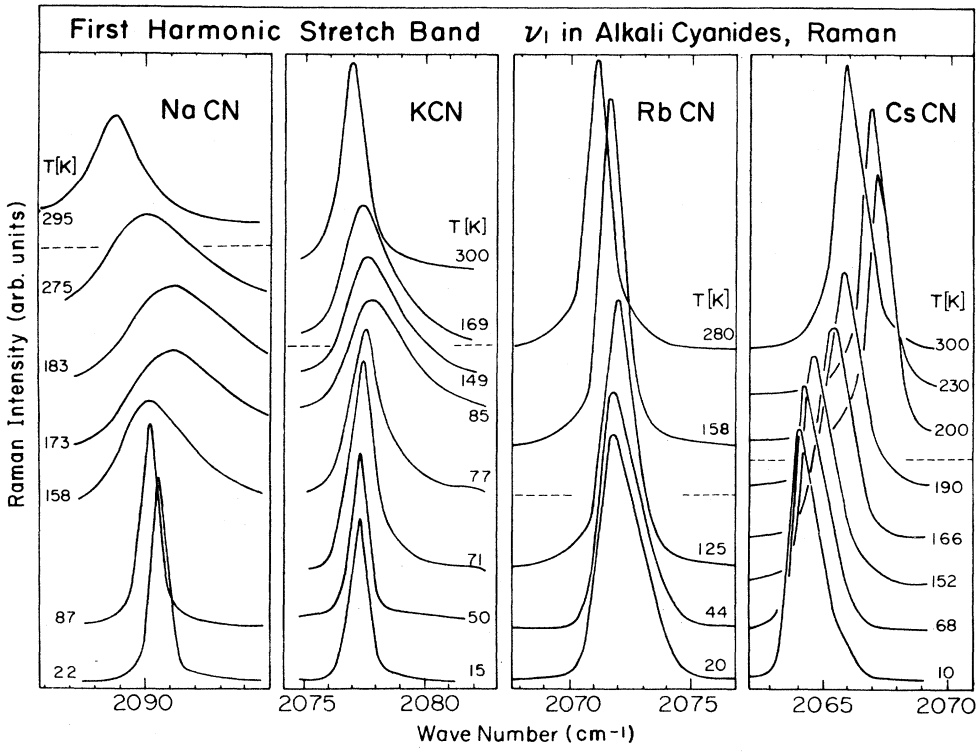

FIG. 3. Raman spectra of the first harmonic CN^- stretching response, measured in four pure alkali cyanide crystals at various temperatures.

the two materials (KCN and NaCN) with known low-temperature electric ordering the width starts to decrease at T_{C2} and reaches again very small values at lowest temperatures; for the two materials with no electric ordering (RbCN and CsCN) this additional low temperature narrowing effect is missing.

An extremely weak second harmonic of the CN^- stretching (never before observed in Raman scattering) could be measured in NaCN, KCN, and RbCN. The band is barely above the detection limit, being a factor of about 10^4 less intense than the first harmonic, and is therefore essentially only observable in the high temperature (transparent) crystal phase. Only in KCN, where stress alignment of domains allows effective reduction of the crystal opacity,[18] the weak second harmonic band could be followed partially to low temperatures. The position of the second harmonic band in the three investigated materials was found to lie by 22.0 ± 1.1 cm^{-1} below the double value of the first-harmonic vibration.

As expected, the first harmonic stretching band is always accompanied by two small satellite bands produced by the stretching motion of $^{13}C\,^{14}N$ and $^{12}C\,^{15}N$ molecules, appearing with a relative strength given by the material isotope ratio (1.1% for ^{13}C and 0.37% for ^{15}N).

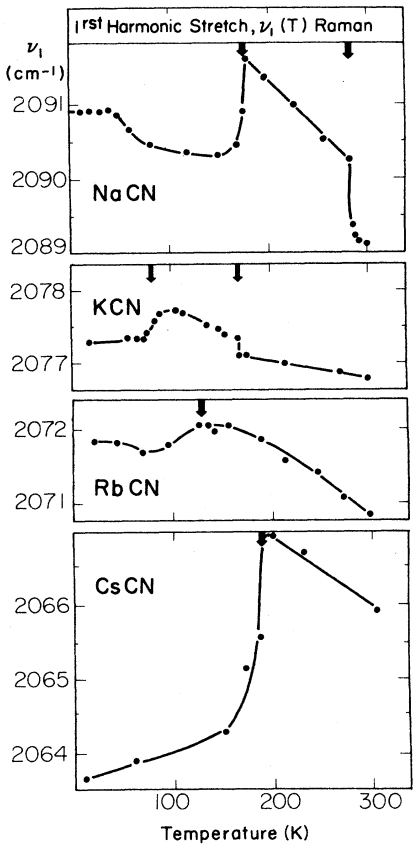

FIG. 4. Peak position ν_1 of the first harmonic CN^- stretching band, measured with Raman techniques for alkali cyanide crystals as a function of temperature.

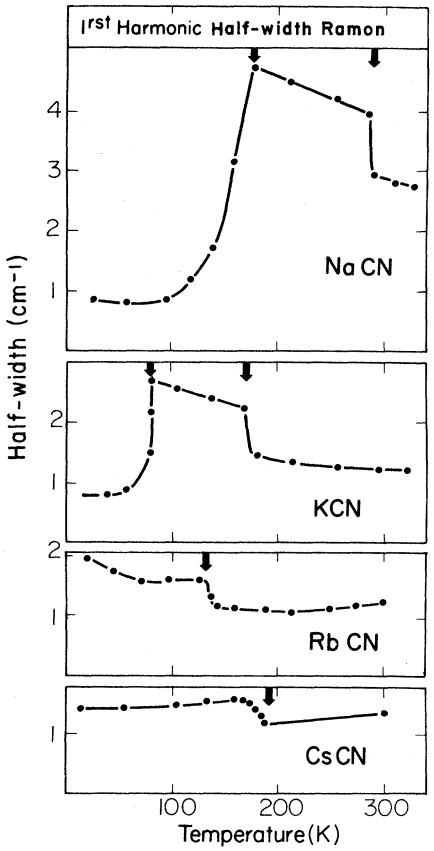

FIG. 5. Half-width of the first harmonic CN^- stretching band, measured with Raman techniques in four alkali cyanide crystals as a function of temperatures.

These isotope bands behave under temperature variation like small replicas of the main $^{12}C\,^{14}N$ band with similar broadening and shift effects, and with relative positions very close to the ones predicted by the ratio of the reduced masses. All relevant Raman data are summarized in Table I.

B. Infrared results

The first harmonic stretching band is by far too strong to be analyzed by absorption spectroscopy. Therefore, in the *first harmonic region* only the small isotope lines from $^{13}C\,^{14}N$ and $^{12}C\,^{15}N$ molecules could be measured with ir spectroscopy, while the position of the first harmonic could be inferred from these isotope data only approximately using the peak position ratio obtained by Raman measurements in the fundamental band.

Most infrared data were therefore taken in the *second harmonic region,* where the absorption is about 125 times less intense compared to the one in the fundamental region. Figure 6 gives a summary of a selection of second harmonic spectra measured in the four materials at various temperatures. The considerable variations in area (A), peak position (ν), and width (H), showing up in this summary, are plotted separately as a function of tempera-

TABLE I. Absolute and/or relative values of the frequency (ν) and strength (I) of first, second, and third harmonic CN^- transition in four pure alkali cyanides, measured with ir and Raman at liquid-helium temperatures LHeT. [Exceptions, measured at RT, are marked with an asterisk (*).] The intensity of the first harmonic ir transition (**) has been calculated from the abundance ratio of the measured isotope stretching absorption. All frequency (ν) values are given in (cm^{-1}) units.

CN^-	Quantities	Technique	NaCN	KCN	RbCN	CsCN
First	$\nu_1^{12,14}$	Raman*	2089.1	2076.7	2070.8	2065.9
harmonic	$\nu_1^{12,15}$	Raman	2059.4	2045.9	2040.9	2031.7
		ir	2057.0	2044.7	2039.0	2032.0
	$\nu_1^{13,14}$	Raman	2048.2	2034.8	2029.2	2021.4
		ir	2045.8	2034.5	2027.5	2021.3
	$\nu_1^{12,14}/\nu_1^{12,15}$	Raman	1.0153	1.0153	1.0152	1.0157
	$\nu_1^{12,14}/\nu_1^{13,14}$	Raman	1.0208	1.0209	1.0210	1.0209
Second	$\nu_2^{12,14}$	Raman*	4156.1	4130.4	4119.5	
harmonic		ir*	4155.6	4130.6	4120.7	4106.8
	$\nu_2^{12,15}$	ir	4093.7	4069.2	4058.4	4040.4
	$\nu_2^{13,14}$	ir	4071.2	4046.9	4035.5	4017.2
	$\nu_2^{12,14}/\nu_2^{12,15}$	ir	1.0153	1.0151	1.0154	1.0152
	$\nu_2^{12,14}/\nu_2^{13,14}$	ir	1.0209	1.0210	1.0211	1.0211
	$(2\nu_1-\nu_2)^{12,14}$	ir*	22.6	22.8	22.1	25.0
		Raman*	22.1	23.0	20.9	
	I_1/I_2	ir**	115±7%	120±7%	105±7%	125±7%
		Raman*	~10000	~5000	~5000	
Third	$\nu_3^{12,14}$	ir*	6196.3	6159.9	6142.5	6123.9
harmonic	$(3\nu_1-\nu_3)^{12,14}$	ir*	71.0	70.2	69.9	73.8
	I_2/I_3	ir*	160±10%	190±10%	170±10%	125±10%

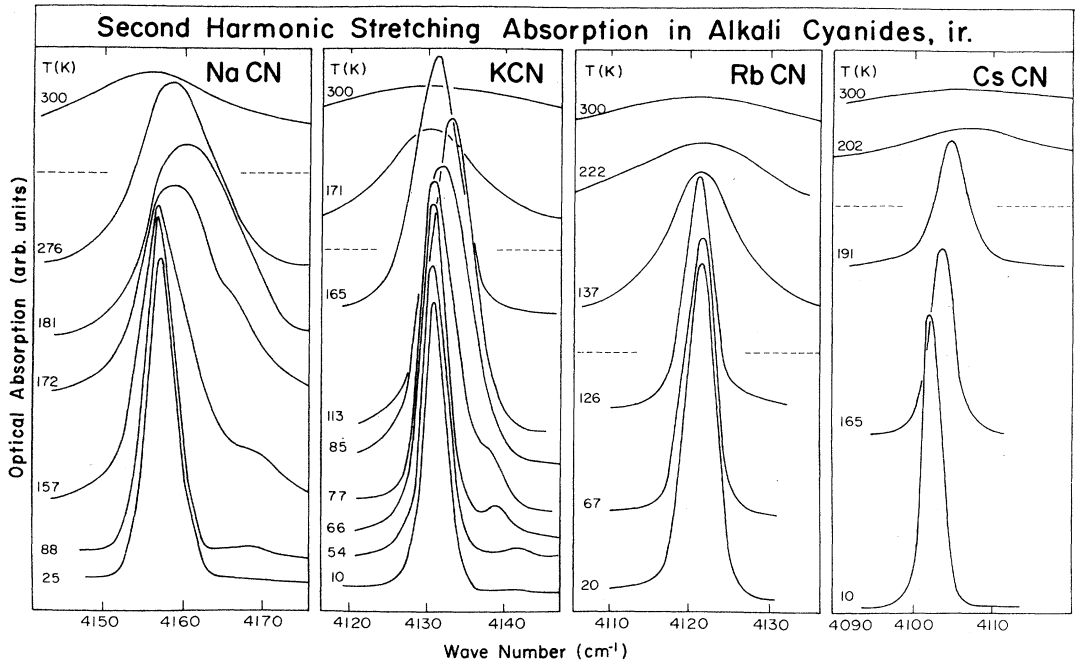

FIG. 6. Infrared spectra of the second harmonic stretching absorption in four alkali cyanide materials at various temperatures.

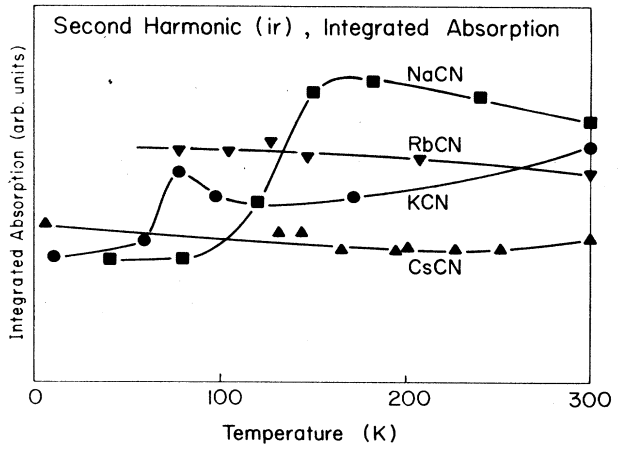

FIG. 7. Integrated area (A) of the ir second harmonic stretching absorption (in an arbitrary but common scale) as a function of temperature in four alkali cyanides.

ture in Figs. 7–9, respectively. Similar to the Raman case (Figs. 4 and 5) all the known critical temperatures T_{C1} and T_{C2} (indicated by arrows) show up as distinct changes in the values or slopes of $A(T)$, $\nu(T)$, and $H(T)$ curves. [The only exception is RbCN where the changes

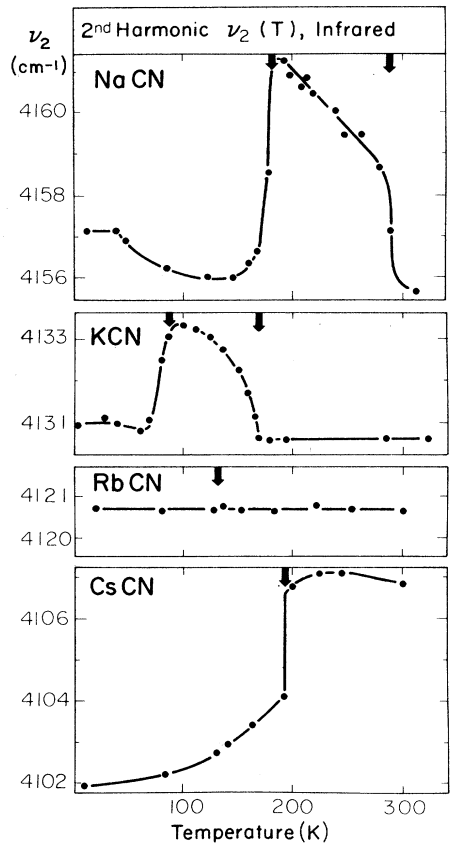

FIG. 8. Peak position of ir second harmonic stretching absorption (ν_2) as a function of temperature in four alkali cyanides.

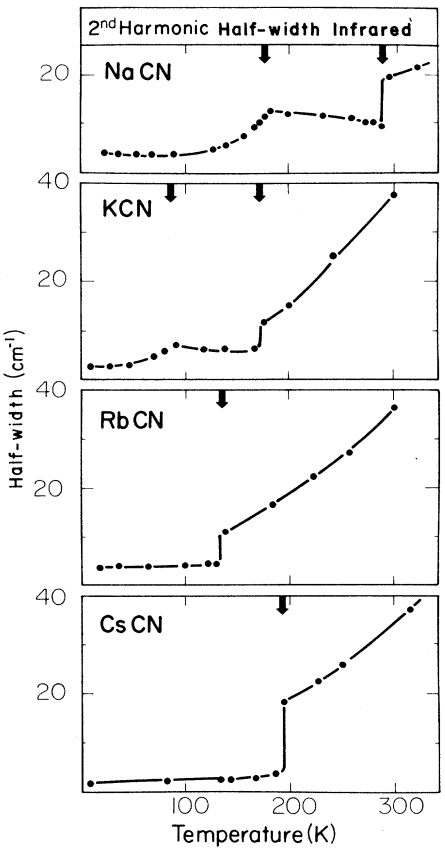

FIG. 9. Half-width of the ir second harmonic stretching absorption (ν_2) as a function of temperature in four alkali cyanides.

of $\nu(T)$ at T_{C1} both in Raman and infrared are minute.] The biggest general difference to the Raman case is the very *large width* in the high-temperature phase, which *decreases* under cooling and drops abruptly at T_{C1} (while in Raman the small width at high temperatures *increases* abruptly at T_{C1} to a value about half of the ir overtone). Many other features, however, like the gradual narrowing and low-energy shift under cooling of KCN and NaCN below T_{C2} into the range of electric ordering, are very similar in Raman and infrared measurements. The additional data on the integrated ir response (not taken in Raman) show a decrease below the antiferroelectric ordering temperature T_{C2}.

The difference between the second harmonic peak position and the double of the first harmonic position is rather constant among all the substances and phases, with a value of 23.5 ± 1.5 cm^{-1}. The weak satellite absorptions due to ^{13}C and ^{15}N isotopes show, like in Raman, a replica behavior compared to the main band; which in terms of the $\nu(T)$ behavior is illustrated in Fig. 12 (presented later).

In the third harmonic region (~ 6000 cm^{-1}), a very weak absorption band could be detected in all four materials, about a factor of 170 smaller in integrated intensity than the second harmonic band. The observed peak position of these bands is about 70 cm^{-1} less than three

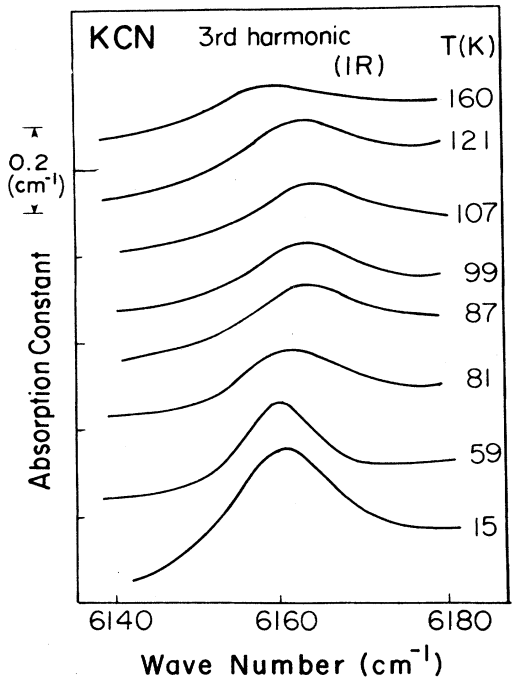

FIG. 10. Infrared spectra of the third harmonic CN^- stretching absorption (ν_3) in KCN, measured at various temperatures.

times the value of the first harmonic. Figure 10 shows the spectrum of the weak third harmonic and its temperature dependence for KCN, while Fig. 11 shows the $\nu_3(T)$ dependence for both KCN and NaCN. Both the

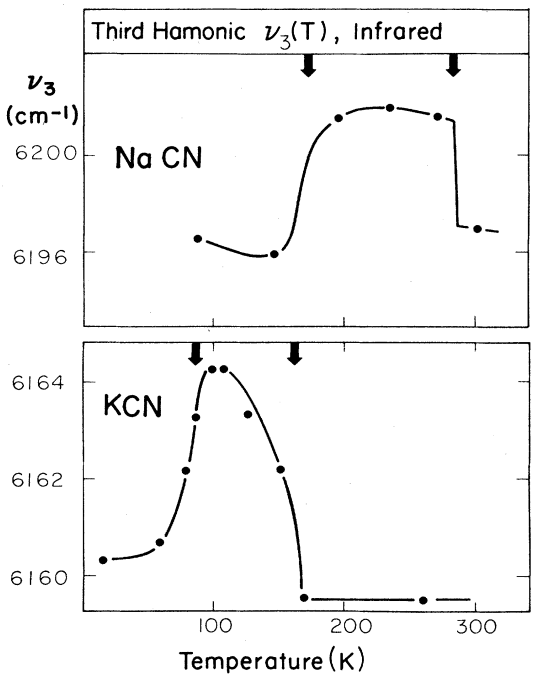

FIG. 11. Peak position of the infrared third harmonic CN^- stretching band (ν_3) in NaCN and KCN, as a function of temperature.

$\nu(T)$ pattern and the half-width variation with temperature (not quantitatively measured due to the necessary large spectral slitwidth) are found to be very much parallel to the ones of the second harmonic. All relevant numerical data of the ir measurements are summarized (and compared to the Raman data) in Table I.

C. Spectral sidebands

A variety of sidebands originating from different physical phenomena are observed close to the main vibrational transitions discussed so far.

(a) As mentioned already above, *isotope satellites* due to $^{13}C\,^{14}N$ and $^{12}C\,^{15}N$ molecules appear on the low-energy side of the Raman and ir transitions, with a strength expected from the natural isotope ratio and relative position close to the ones predicted by the reduced mass ratio.

(b) On the high-energy side of the first harmonic ir transitions a sideband spectrum extending over a 200–300 cm^{-1} range appears with a strength similar to the isotope satellites. It is due to *combinations of stretching and libration-rotation excitations* of the CN^- system and has been already treated and analyzed.[19]

(c) In all four cyanides, a sideband has been found in the second harmonic ir spectrum (missing in the first harmonic range), located at 24.3 ± 1.5 cm^{-1} above the main band ν_2 at exactly the double frequency $2\nu_1$ of the first

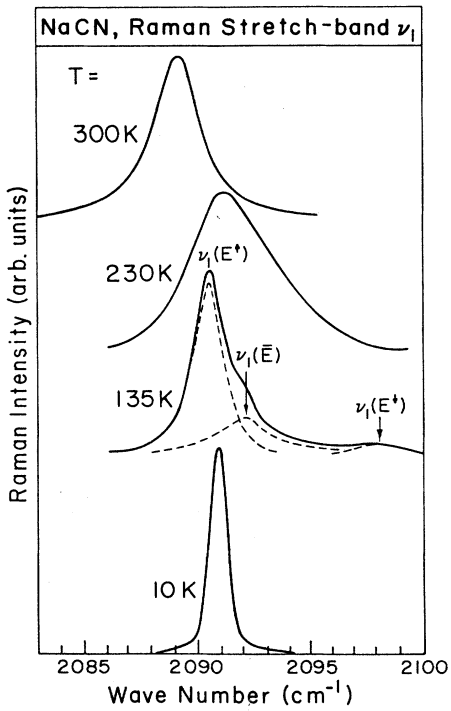

FIG. 12. Raman spectra of the first harmonic CN^- stretching response (ν_1) measured in NaCN at four selected temperatures. The spectral main-band and sideband structure, appearing at $T=135$ K, and its notation "$\nu_1(E^\uparrow)$, $\nu_1(\bar{E})$, and $\nu_1(E^\downarrow)$," will be discussed in Sec. III.

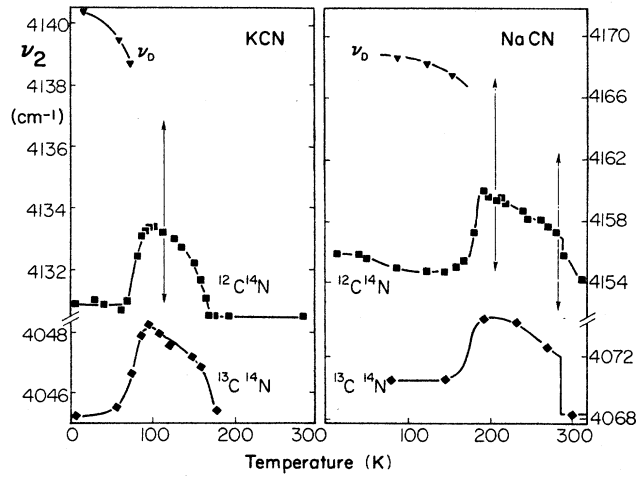

FIG. 13. Peak position of the second harmonic CN^- stretching absorption bands (ν_2) (for $^{12}C^{14}N$ and $^{13}C^{14}N$) together with the position of the sideband $\nu_2(E^{\downarrow})$ as a function of temperature.

harmonic. This has been analyzed and interpreted previously as a *cooperative absorption* of a single photon by a pair of interacting CN^- molecules, exciting both to the first excited vibrational state.[26]

Besides these well understood and previously discussed effects (a)–(c), a new type of sideband was observed in this work. It is present only in KCN and NaCN at low temperatures and can at least partially be seen in the surveys of Figs. 3 and 6. Under cooling below T_{C1} through the elastically ordered phase, both the Raman and ir stretching bands become increasingly unsymmetric with a long extended tail on the high-energy side. Under further cooling beyond T_{C2}—the onset of antiferroelectric ordering—this high-energy tail develops spectral structure in the form of distinct sidebands (two resolved in Raman and one in ir measurements). These sidebands display increasing separation and steadily decreasing strength and disappear totally at lowest temperature when full electric order is achieved. Figure 12 illustrates for NaCN this appearance of unsymmetry, its development into sideband structure, and their total disappearance at four selected temperatures under successive cooling. (A similar splitting into three components with less separation and resolution is observed in Raman for KCN.) Figure 13 shows the temperature dependence of the peak position of the only sideband resolved with ir techniques, in comparison to the position of the second harmonic stretching bands (for $^{12}C^{14}N$ and $^{13}C^{14}N$). This new type of sideband with *strongly temperature dependent position and strength,* occurring only for NaCN and KCN in the temperature range of partial electric order, will play an important part in our discussions.

III. DISCUSSION AND MODELS

We have to construct and discuss models for the CN^- stretching mode, which are able to explain the optical behavior, observed with ir and/or Raman techniques, in four host materials and their different phases. The essential features, to be treated and explained, include energy position, strength, and bandwidth of the first, second, and third harmonics and their variation with host and phase changes. The model will proceed from a simple harmonic one to an anharmonic model based on "mechanical" and "electrical" anharmonicity, and will take into account the effects of the local static electric field from antiferroelectric ordering on the harmonic transitions.

A. Host material variation of the first harmonic mode

The first harmonic stretching frequency ν observed for CN^- in alkali halide and alkali cyanide hosts depends, as already mentioned, systematically on the lattice spacing of the host, which can be regarded as an hydrostatic pressure or A_{1g} deformation acting on the CN^- molecule. This naturally raises the question, if a purely experimental relation, like the Ivey law for F centers in alkali halides,[27] can be formulated for the CN^- stretching frequency. We attempt this by arguing[24] that the eigenfrequency ν_f of a completely free unconfined CN^- molecular ion becomes shifted increasingly to higher values, if the CN^- ion is confined into hosts of decreasing lattice parameter d (or cell volume V). For a power-law dependence we could expect a relation of the form

$$\nu-\nu_f=kV^{-x}\,. \tag{1}$$

A relation of this type can be verified only in two steps: by assuming a "reasonable" exponent x (like $x=0.5$ or 1.0) and plotting the observed ν values in a linear scale versus V^{-x}, one obtains a nonstraight line dependence which can be extrapolated to $V\to\infty$, yielding a value for ν_f. Doing this for ν values in the NaCl structure we obtain (rather independent of the chosen x) $\nu_f\approx 2000$ cm^{-1}. With this obtained ν_f value one can then plot $(\nu-\nu_f)$ versus V in a double logarithmic scale, and the exponent x is determined from the slope, if a straight line dependence is observed.

The most simple choice for the volume V in which the CN^- ion is confined is the volume of the cation-anion pair, which is $V=2a^3$ for the NaCl structure and $V=a^3$ for the CsCl structure (a is interionic distance). Figure 14 shows the result of such a plot, using $\nu_f=2000$ cm^{-1}. Both NaCl and CsCl structure data fall on a reasonable good straight-line dependence (within $\Delta\nu_f=\pm 3$ cm^{-1}) yielding a slope of about $x=\frac{2}{3}$. Translated from volume V to lattice parameter d (by $V\propto d^3$) this produces indeed an Ivey-type law of the familiar dependence on d^{-2}. By using instead of the cation-anion-pair volume different types of "available volumes" for the CN^- ion we could improve the straight-line dependence, but without any significant changes in the parameters ν_f, x, and k. We will thus accept the empirical relation

$$\nu-\nu_f=kV^{-2/3} \tag{1'}$$

with $\nu_f=2002$ cm^{-1} and $k=1.3\times10^{-13}$ cm. It should be noted that Field and Sherman[24] have attempted to derive similarly an "universal" plot of the CN^- first harmonic frequencies ν in various hosts compared to the

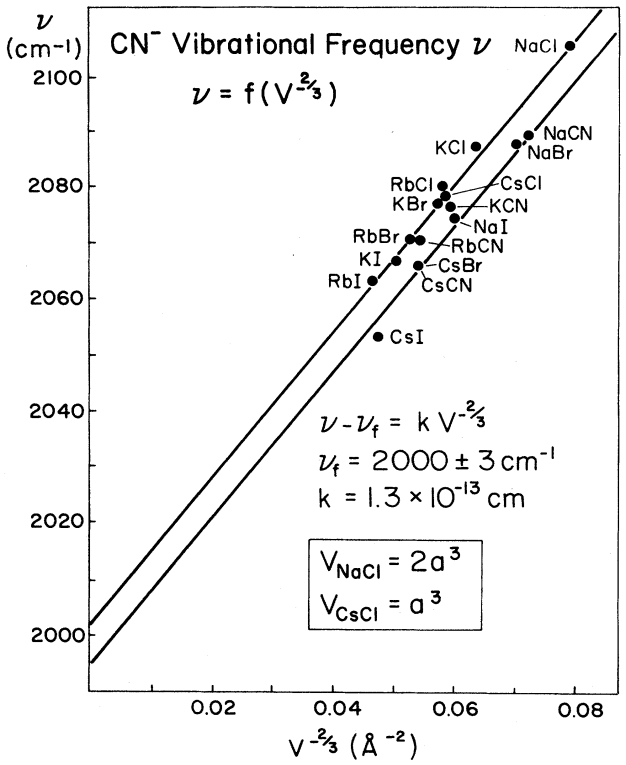

FIG. 14. Fundamental stretching frequency ν of CN^- defects in 12 alkali halides and of three pure alkali cyanides plotted against $V^{-2/3}$ (V is volume available for the CN^- molecule in the host), showing an approximate "Ivey-law" behavior (see text).

free-ion value ν_f based on calculations of the interaction energies between CN^- and the surrounding lattice. Their best value for ν_f is 2038 cm^{-1}, far outside the value obtained with our simple Ivey-type law, indicating that the interaction energy which shifts the stretching frequency could be underestimated in their calculation.

At the elastic phase transition we observe (Figs. 4 and 8) a peak position shift related to the cubic (unordered)↔elastically ordered phase transition. It is interesting to check if this shift can—at least roughly—be explained by the model presented here: the empirical $V^{-2/3}$ relation predicts that small volume change ΔV of a host should produce stretching frequency shift $\Delta\nu$ according to

$$\frac{\Delta\nu}{\nu-\nu_f}=-\frac{2}{3}\frac{\Delta V}{V}. \tag{2}$$

From x-ray or neutron diffraction data the relative change $\Delta V/V$ of the volume of the unit cell at the elastic phase transition has been evaluated for the different pure alkali cyanides. These results are listed and compared with $\Delta\nu/(\nu-\nu_f)$ in Table II. Three cases must be differentiated.

(a) In NaCN and KCN the cubic→orthorhombic transition produces the expected high-energy shift of the stretch mode, however of a size somewhat smaller than

TABLE II. Relative change in volume $\Delta V/V$ and stretching frequency ($\Delta\nu/\nu-\nu_f$) at the elastic phase transition of pure alkali cyanides.

Crystals	$-\frac{2}{3}\Delta V/V$	$\Delta\nu/\nu-\nu_f$
NaCN	<2.4% [a]	1.3%
KCN	<1.1% [b]	0.33%
RbCN	~0.1% [c]	~0
CsCN	0.5% [d]	−2%

[a]From Ref. 13.
[b]From Ref. 12.
[c]From Ref. 5.
[d]From Ref. 6.

predicted by Eq. (2) of the simple isotropic contraction model. The deviation is evidently caused by the anisotropy of the lattice contraction and CN^- molecule orientation, the latter aligned parallel to the direction of largest ionic separation.

(b) In RbCN the cubic→monoclinic (antiferroelastic) transition produces nearly no volume change, in agreement with the absence of stretching band shift.

(c) In CsCN the cubic→rhombohedral (ferroelastic) transition[6] produces a volume contraction in spite of which a considerable low-energy shift of the stretch band occurs. This apparent contradiction to Eq. (2) can however be explained: the trigonal deformation around the ⟨111⟩ axes of the cubic cell reduces the angle from 90° to 87° and the volume of the cell by 0.8%, but simultaneously elongates the ⟨111⟩ body diagonal (along which the CN^- molecules become aligned) by about 4%. This qualitatively explains reduction in repulsive interaction and low-energy shift of the CN^- stretch band.

Careful measurements of the relative peak positions of the isotopic bands $\nu^{12,15}$ and $\nu^{13,14}$ with respect to the main band $\nu^{12,14}$ both in Raman and ir, show systematic deviation from the theoretical value calculated—for totally uncoupled molecules—from the square root of the reduced mass ratio. This deviation appears to be rather constant and independent of temperature, phase, substance, and measurement techniques, making the isotope shift (Table I) consistently smaller (about 1 cm^{-1}) than the theoretical value. For explanation, we can regard the rare isolated isotopic molecules to be slightly dynamically coupled to (or "dressed by") the abundant surrounding $^{12}C\,^{14}N$ neighbors, so that the latter participate slightly in the molecular vibration of the isotopic CN^- molecule. This dressing effect, however is extremely small (0.05% deviation from the theoretical isotope shift). As expected, no deviation from the theoretical value is observable in the frequency positions of the two isotopic $^{12}C\,^{15}N$ and $^{13}C\,^{14}N$ stretching bands with respect to each other.

B. Mechanical anharmonicity model

The existence of higher harmonics of the CN^- stretching mode observed in infrared and Raman confirms the necessity to assume a "mechanical" anharmonicity for

the CN^- molecule. The rather constant overtone frequency shift from a multiple value of the 1st harmonic—under variations of both the host and the CN^- concentration—shows that the mechanical anharmonicity is a property related essentially to the CN^- molecule alone.

1. Frequencies of the harmonics

The vibrational energy levels are obtained by solving the Schrödinger equation for a given potential $U(r)$

$$\frac{d^2\psi(r)}{dr^2}+\frac{2\mu}{h^2}[E_{\text{vib}}-U(r)]\psi(r)=0 \tag{3}$$

or

$$\frac{d^2\psi(\xi)}{d\xi^2}+\frac{2\mu r_e^2}{h^2}[E_{\text{vib}}-U(\xi)]\psi(\xi)=0\ , \tag{4}$$

where $\xi=(r-r_e)/r_e$ represents the relative change in interatomic distance around the equilibrium position r_e, and μ is the reduced mass of the oscillator.

One assumes that the molecule experiences an internuclear potential well $U(r)$ containing higher than quadratic perturbation terms of the interatomic distance. The expansion of the potential function about the equilibrium position can be written as

$$U(\xi)=\tfrac{1}{2}k_e r_e^2(\xi^2+a_1\xi^3+a_2\xi^4+\cdots)\ , \tag{5}$$

where $k_e=4\pi^2\nu_e^2\mu$ is the force constant of the oscillator for very small amplitudes and ν_e the corresponding frequency. The eigenvalues of the solutions of the Schrödinger equation or vibrational-energy levels of the molecule are usually written as[28]

$$h\nu(n)=h\nu_e(n+\tfrac{1}{2})-h\nu_e x_e(n+\tfrac{1}{2})^2+\cdots\ , \tag{6}$$

where n is the quantum number and x_e the anharmonicity term (x_e positive $\ll 1$). The sign of x_e is chosen positive in agreement to the sign of a_1 in the power expansion of the potential function [Eq. (5)]. The zero-point energy of the anharmonic oscillator is obtained by putting $n=0$ into Eq. (6), and the 1st harmonic stretching vibration energy $h\nu_1$ is thus given by

$$h\nu_1=h\nu(1)-h\nu(0)=h\nu_e(1-2x_e)\ . \tag{7}$$

Harmonic energies are given by

$$h\nu_n=nh\nu_e[1-(n+1)x_e]\ .$$

The anharmonicity parameter x_e can be obtained from the following equation:

$$n(n-1)h\nu_e x_e=nh\nu_1-h\nu_n\ . \tag{8}$$

In order to solve the energy formula (6), a perturbation calculation procedure must be carried out. Fues[29] and Kemble,[30] using this technique, have shown that

$$x_e=\frac{3}{4}\frac{h\nu_e}{k_e r_e^2}\left[\frac{5a_1^2}{4}-a_2\right]\ . \tag{9}$$

For the description of weakly anharmonic oscillators one often uses in molecular physics the so-called "Morse potential" defined by

$$U_m(\xi)=U_D[1-\exp(-\beta\xi)]^2\ , \tag{10}$$

where U_D is the dissociation energy and β a parameter to be fitted to experimental data. Expanding the Morse potential up to terms of fourth power relates it to the potential $U(\xi)$ of Eq. (5) by the relations

$$\tfrac{1}{2}k_e r_e^2=U_D\beta^2,\quad \tfrac{1}{2}k_e r_e^2 a_1=-U_D\beta^3,\quad \tfrac{1}{2}k_e r_e^2 a_2=\tfrac{7}{12}U_D\beta^4 \tag{11}$$

or

$$\beta=-a_1,\quad U_D=\frac{1}{2}\frac{k_e r_e^2}{a_1^2},\quad \frac{a_2}{a_1^2}=\tfrac{7}{12}\ . \tag{12}$$

For the Morse potential the cubic and quartic anharmonicity terms are not independent [like in Eq. (5)], but numerically related by Eq. (12). Using Eqs. (9) and (12) one also obtains

$$a_1^2=\beta^2=\frac{2k_e r_e^2 x_e}{h\nu_e}\quad\text{and}\quad U_D=\frac{h\nu_e}{4x_e}\ . \tag{13}$$

2. Comparison with experimental data

First and second harmonic peak positions observed by ir or Raman techniques in the different materials are summarized in Table I. We can deduce the anharmonicity parameter using Eq. (8) which yields for the second and third harmonics:

$$2h\nu_e x_e=2h\nu_1-h\nu_2=22.6\ \text{cm}^{-1}\ ,$$
$$6h\nu_e x_e=3h\nu_1-h\nu_3=71.2\ \text{cm}^{-1}\ ,$$

averaged over the four materials. Using the mean value $h\nu_e x_e=11.5\ \text{cm}^{-1}$ and Eq. (7) with $h\nu_1=h\nu_f=2002\ \text{cm}^{-1}$ (the value of the stretching frequency for free CN^- molecule in infinite volume, see Sec. III A), we find $h\nu_e=2025\ \text{cm}^{-1}$ and $x_e=5.6\times10^{-3}$. This leads, with $r_e=1.19$ Å and $\mu=6.46$ amu to $k_e=1.56\times10^6\ \text{erg/cm}^2$ and $h\nu_e/k_e r_e^2=1.83\times10^{-3}$. Using the Morse potential for fitting the experimental results, we obtain from Eq. (13) an averaged parameter $\beta=2.49$ and a dissociation energy $U_D=11.0$ eV. These experimental values are reported in Table III and are compared with calculated ones found in the literature. Transposition of these results for corresponding frequencies of CN^- stretching mode in host materials like alkali cyanide is straightforward.

3. Relative intensities of the harmonic transitions

We have to distinguish between ir and Raman measurements. In order to calculate the ir intensities of the harmonics one must know the matrix component P_n of the electric moment associated with the absorption transition $0\rightarrow n$

$$P_n=\int p(r)R_0(r)R_n(r)dr\ , \tag{14}$$

TABLE III. Comparison between CN^- experimental data and values calculated in different theoretical papers.

CN^- Quantities	Experimental data	Theoretical values
Anharmonic constant $h\nu_e x_e$	11.5 cm^{-1}	11.3 cm^{-1} (Ref. 35)
Fundamental harmonic frequency ν_e	2025 cm^1	2193 cm^{-1} (Ref. 33) 2038 cm^{-1} (Ref. 24) 2150 cm^{-1} (Ref. 35)
Force constant k_e	1.56×10^6 erg/cm^2	1.83×10^6 erg/cm^2 (Ref. 33) 1.63×10^6 erg/cm^2 (Ref. 24)
Anharmonic potential a_1	−2.49	−2.43 (Ref. 33)
parameters a_2	3.62	4.02 (Ref. 33)
Dissociation energy V_D (Morse potential)	11.0e Å	10.45 (Ref. 35)
Dipole moment of CN^-	0.07e Å	0.078e Å (Ref. 33) 0.13e Å (Ref. 35)
Dipole moment gradient dp/dr	|0.26|e	−0.48e (Ref. 33)
Polarizability α_{zz}		$2.5\times10^{-4}e$ $Å^2$/V (Ref. 33)
Polarizability gradient $d\alpha/dr$		0.32e Å/V (Ref. 33)
$\frac{d^2p}{dr^2}\Big/\frac{dp}{dr}$	−0.49 $Å^{-1}$	
$\frac{d^2\alpha}{dr^2}\Big/\frac{d\alpha}{dr}$	+2.3 $Å^{-1}$	
Static electric field in antiferroelectric phase		
E (NaCN)	2.45×10^7 V/cm	4.79×10^7 V/cm (Ref. 34)
E (KCN)	1.56×10^7 V/cm	1.56×10^7 V/cm (Ref. 34)

where $R(r)$ is the radial P part of the wave function. Expanding the electric moment $p(r)$ in a power series about the equilibrium point

$$p(\xi)=p_e+p_e'\xi+\frac{p_e''}{2}\xi^2+\cdots, \tag{15}$$

where

$$p_e'=\left[\frac{dp}{d\xi}\right]_{\xi=0},$$

etc. Dunham (31) has shown that the intensity ratio between the first and second harmonics is given by

$$\frac{I_2}{I_1}=\frac{\nu_2}{\nu_1}\left[\frac{P_2}{P_1}\right]^2. \tag{16}$$

Ignoring terms of order higher than ξ^2 in the power expansion of the electric moment $p(r)$, this reduces to the following equation

$$\frac{I_2}{I_1}(\text{ir})\simeq\frac{1}{2}\frac{h\nu_e}{k_e r_e^2}(a_1+\rho)^2, \tag{17}$$

where

$$\rho=\frac{d^2p(r)}{d\xi^2}\Big/\frac{dp(r)}{d\xi}=r_e\frac{d^2p(r)}{dr^2}\Big/\frac{dp(r)}{dr}. \tag{18}$$

If we assume that the Raman intensity is given by the same kind of equation as for ir [Eq. (17)] in which the polarizability component (A) derivatives replace the dipole moment (ρ) derivatives, we can write

$$\frac{I_2}{I_1}(\text{Raman})\simeq\left[\frac{\lambda_1}{\lambda_2}\right]^4\frac{h\nu_e}{k_e r_e^2}(a_1+A)^2, \tag{19}$$

where λ_1 and λ_2 are the wavelengths at which the first and second harmonics are recorded in Raman scattering (λ_1 and λ_2 are depending on the laser excitation wavelength). A has the same meaning as ρ [Eq. (18)] translated for Raman

$$A=r_e\frac{d^2\alpha}{dr^2}\Big/\frac{d\alpha}{dr} \tag{20}$$

(with α the polarizability along the molecule axis).

4. *Comparison with experimental data*

The ir intensity ratio I_2/I_1 is rather constant over all the host materials and phases (see Table III). Using Eq. (17) we deduce

$$(a_1+\rho)^2=9.5.$$

a_1 must be negative due to the shape of the internuclear potential and according to Eqs. (12) we obtain

$$a_1=-2.49,\quad a_2=3.62,\quad \rho=+5.57 \text{ or } -0.59.$$

It is reasonable to assume that $|\rho|$ is small, so that only the negative value of ρ makes sense. From Eq. (18) we obtain

$$\frac{d^2p(r)}{dr^2}\Big/\frac{dp(r)}{dr}=-0.49\ Å^{-1}.$$

The Raman 2nd harmonic intensity is definitely lower than the ir one compared to the 1st harmonic (by a factor of ~100). From the observed Raman second harmonic intensity and use of Eq. (19) one gets $A\simeq2.8$ with a positive sign (opposite to ρ in order to decrease the calculated

intensity), which leads to

$$\frac{d^2\alpha}{dr^2}\Big/\frac{d\alpha}{dr}=2.3\ \text{Å}^{-1}\ .$$

These results are summarized in Table III.

C. Anharmonicity in the presence of a static electric field

The existence of an intense electric field building up below T_{C2} in the antiferroelectric phase of NaCN and KCN induce two experimentally observed phenomena.

(a) A decrease of the total integrated intensity of the ir second harmonic (see Fig. 7) below T_{C2} when cooling the sample.

(b) A shift of the first and second harmonics of the stretching mode (Figs. 4, 6, 8, and 13) towards low energy, accompanied in the ir second harmonic as well as in the Raman first harmonic by the formation of a stretching satellite $\nu_n(E^{\downarrow})$ ($n=1$ or 2) (Figs. 6, 12, and 13) which shifts towards high energy but decreases in intensity towards lower temperature. These satellite first and second harmonic bands are attributed to transitions from the counteraligned ($E^{\downarrow}$) CN^- molecules with respect to the main electric field ($E^{\uparrow}$). Their number is decreasing with decreasing temperature while the main ($E^{\uparrow}$) electric field augmentation increases the observed splitting. The third band resolved in the first harmonic Raman response and called $\nu_1(\bar{E})$ in Fig. 12 is assumed to be due to Raman transitions of CN^- dipoles occupying intermediate (nonaligned) orientations in respect to the electric field.

According to Gready, Bacskay, and Hush[32] a model can be developed for interpreting and evaluating peak position shift of harmonic stretching vibrations for isolated CN^- molecule under static electric field.

1. Intensity variation of ir transition

The presence of a static electric field induces extra dipole moment to the molecule according to

$$p(E)=p(0)+\alpha E\ , \tag{21}$$

where α is the polarizability tensor component along the dipole axis and $p(E)$ the dipole moment of CN^- in the presence of the static electric field. Thus $dp/dr=p'$ is given by

$$p'(E)=p'(0)+\alpha' E\ . \tag{22}$$

The $\alpha' E$ term in Eq. (22) modifies the intensity of the ir second harmonic under cooling (Fig. 7), when an electric field is building up. The relative variation in the intensity of the second ir harmonic is given by

$$\frac{I_2(E)}{I_2(0)}=\left[\frac{p'(E)}{p'(0)}\right]^2=\left[\frac{p'(0)+\alpha' E}{p'(0)}\right]^2=\left[1+\frac{\alpha' E}{p'(0)}\right]^2 \tag{23}$$

the observed decrease in intensity indicates that $p'(0)$ and α' must have opposite sign.

2. Mode splitting and frequency shift

Regarding $p(E)$ as the CN^- dipole moment including the extra dipole induced by the electric field E, its interaction energy with the field is given by

$$W(E)=-\int p(E)dE\ . \tag{24}$$

If E is directed along the CN^- molecular axis, relation (24) can be reexpressed using Eq. (21) so that

$$W(E)=-p(0)E-\tfrac{1}{2}\alpha E^2\ . \tag{25}$$

One has to notice that the theory of Gready, Bacskay, and Hush (Refs. 32 and 33) used the opposite sign convention in expressing the interaction energy $W(E)$ of an electric dipole with a static electric field, directed along the molecular axis of the dipole. This will be taken into account when we compare later our experimental results with their calculations. Both α and $p(0)$ are dependent on r. Expending the total interaction energy in a Taylor's series about r_e one gets

$$U(E)=\tfrac{1}{2}k_e r_e^2\xi^2+\tfrac{1}{2}k_e r_e^2 a_1\xi^3+\cdots-E[p_e(0)+p_e'(0)\xi+\tfrac{1}{2}p_e''(0)\xi^2+\tfrac{1}{6}p_e''(0)\xi^3+\cdots]$$
$$-\tfrac{1}{2}E^2[\alpha_e+\alpha_e'\xi+\tfrac{1}{2}\alpha_e''\xi^2+\tfrac{1}{6}\alpha_e''(0)\xi^3+\cdots]\ . \tag{26}$$

One notices that $U(E)$ contains now terms constant and linear with the internuclear coordinates which produce a shift of the potential minimum given in first approximation by

$$\delta r_e(E)\simeq+\frac{1}{r_e k_e}[Ep_e'(0)+\tfrac{1}{2}E^2\alpha_e']\ . \tag{27}$$

Calculating the parameters of this new potential with shifted equilibrium, we obtain for the field-dependent force constant

$$k(E)|_{r_e+\delta r_e(E)}\simeq k_e+\frac{1}{r_e^2}\{[3a_1p_e'(0)-p_e''(0)]E+\tfrac{1}{2}(3a_1\alpha_e'-\alpha_e'')E^2\}\ . \tag{28}$$

Due to the extremely small effect of the quartic a_2 term on $\delta r_e(E)$, it has been neglected in Eqs. (27) and (28). Within the *harmonic approximation* the vibrational-energy levels with or without electric field are given by

$$h\nu(n,E)=\frac{h}{2\pi}\left[\frac{k(E)}{\mu}\right]^{1/2}(n+\tfrac{1}{2})$$

or (29)

$$h\nu(n,0)=\frac{h}{2\pi}\left[\frac{k(0)}{\mu}\right]^{1/2}(n+\tfrac{1}{2})\ .$$

The transition energies between these energy levels are

given by

$$h\nu_n(E)=h\nu(n,E)-h\nu(0,E) \tag{30}$$

and the following general relation holds for their field effect:

$$h\nu_n(E)=h\nu_n(0)\left[\frac{k(E)}{k(0)}\right]^{1/2}. \tag{31}$$

This yields for the nth harmonic stretching mode

$$h\nu_n(E)=h\nu_n(0)\left\{1+\frac{1}{k_e r_e^2}\{[3a_1 p_e'(0)-p_e''(0)]E+\tfrac{1}{2}(3a_1\alpha_e'-\alpha_e'')E^2\}\right\}^{1/2}, \tag{32}$$

which for

$$\frac{[3a_1 p_e'(0)-p_e''(0)]E+\frac{3}{2}(3a_1\alpha_e'-\alpha_e'')E^2}{k_e r_e^2}\ll 1,$$

can well be approximated by

$$h\nu_n(E)=h\nu_n(0)\left\{1+\frac{1}{2k_e r_e^2}\{[3a_1 p_e'(0)-p_e''(0)]E+\tfrac{1}{2}(3a_1\alpha_e'-\alpha_e'')E^2\}\right\}, \tag{33}$$

which, when using Eqs. (18) and (20) transforms to

$$h\nu_n(E)=h\nu_n(0)\left\{1+\frac{1}{2k_e r_e}[(3a_1-\rho)p'(0)E+\tfrac{1}{2}(3a_1-A)\alpha_e' E^2]\right\}. \tag{34}$$

Thus the nth harmonic stretching mode, under electric field, splits into two components related to aligned ($E^{\uparrow}$) and counteraligned ($E^{\downarrow}$) CN^- molecules with respect to the main ($E^{\uparrow}$) electric field. The splitting energy difference is given by

$$\Delta[h\nu_n(E^{\uparrow\downarrow})]=h\nu_n(E^{\uparrow})-h\nu_n(E^{\downarrow})=+\frac{h\nu_n(0)}{k_e r_e}(3a_1-\rho)p'(0)E^{\uparrow} \tag{35}$$

and the low-energy mode will be related to aligned ($E^{\uparrow}$) CN^- molecules as long as $(3a_1-\rho)p'(0)$ is negative.

The relative shift with respect to the zero-field unsplit $h\nu_n(0)$ transition energy can be evaluated for aligned ($E^{\uparrow}$) CN^- molecules by

$$\frac{\Delta[h\nu_n(E^{\uparrow}0)]}{h\nu_n(0)}=\frac{h\nu_n(E^{\uparrow})-h\nu_n(0)}{h\nu_n(0)}=\frac{+E}{2k_e r_e}[(3a_1-\rho)p'(0)+\tfrac{1}{2}(3a_1-A)\alpha_e' E]. \tag{36}$$

It presents a negative shift (towards low energy) as long as the quantity $[(3a_1-\rho)p'(0)+\frac{1}{2}(3a_1-A)\alpha_e' E]$ is negative. In the same way, for the counteraligned ($E^{\downarrow}$) CN^- molecule we obtain

$$\frac{\Delta[h\nu_n(E^{\downarrow}0)]}{h\nu_n(0)}=\frac{-E}{2k_e r_e}[(3a_1-\rho)p'(0)-\tfrac{1}{2}(3a_1-A)\alpha_e' E]. \tag{37}$$

The two component energy positions $h\nu_n(E^{\uparrow})$ and $h\nu_n(E^{\downarrow})$ are not symmetrically separated from $h\nu_n(\bar{E})$.

Considering the evolution of the aligned ($E^{\uparrow}$) CN^- molecule nth harmonic stretching position under electric field building up process in the antiferroelectric phase below T_{C2}, the slope of the $h\nu_n(E^{\uparrow})$ component with increasing electric field (decreasing temperature) is given by

$$\frac{d}{dE}[h\nu_n(E^{\uparrow})]=+\frac{h\nu_n(0)}{2k_e r_e}[(3a_1-\rho)p'(0)+(3a_1-A)\alpha_e' E]. \tag{38}$$

This slope will be positive when the factor in brackets on the right-hand side of Eq. (38) is positive, thus when

$$E>-\frac{(3a_1-\rho)p'(0)}{(3a_1-A)\alpha_e'}. \tag{39}$$

This value of E does not depend on the alkali cyanide host lattice as long as the parameters a_1, ρ, A, $p'(0)$, and α_e' do not depend on it.

3. *Comparison with experimental data*

In order to use our two main theoretical results [Eqs. (23) and (34)] and their related consequences, we need to know $p_e'(0)$ and α', both in terms of their value and sign. p_e' can be estimated from the intensity of the ir first harmonic stretching mode, but no sign can be obtained from that. From experimental data we find, at room temperature

$$|p'(0)|=0.28e \text{ for KCN},$$

$$|p'(0)|=0.26e \text{ for NaCN}.$$

No quantitative measurements of the Raman intensity have been done in order to obtain α'. Gready, Bacskay, and Hush[33] have calculated both $p'(0)$ and α' (see Table III) and obtained for $p'(0)$ a negative and for α' a positive sign. This opposite sign assumption between p' and α' predicts in Eq. (23) an intensity decrease of the ir stretching harmonics under rising electric field, as we observe (Fig. 7) in KCN and NaCN.

Using our experimental value of $p'(0)$ with a positive sign and the calculated value α' of Ref. 33 (which used opposite sign conventions, as pointed out earlier), we can easily calculate the static electric field existing in the fully ordered antiferroelectric phase of KCN and NaCN at low temperature [Eq. (23)]. We obtain

$$E_{KCN}=1.56\times 10^7 \text{ V/cm},$$

$$E_{NaCN}=2.45\times 10^7 \text{ V/cm}.$$

The splitting of the ir second harmonic into two com-

ponents can be calculated, using Eq. (35) and the different values of $\nu_2(0)$, k_e, r_e, a_1, ρ, $p'(0)$, and E given above and summarized in Table III.

The quantity $(3a_1-\rho)p'(0)$ is found numerically negative. This confirms basically the low-energy shift of the main harmonic mode under antiferroelectric ordering. Assuming that $h\nu_n(\bar{E})\simeq\frac{1}{2}[h\nu_n(E^{\uparrow})+h\nu_n(E_{\downarrow})]$ holds very closely, we find

$$\Delta h\nu_2(E^{\uparrow\downarrow})=-9.9\ \text{cm}^{-1}\ \text{for KCN},$$

$$\Delta h\nu_2(E^{\uparrow\downarrow})=-15.7\ \text{cm}^{-1}\ \text{for NaCN}.$$

These calculated splittings are in correct agreement with the observed ones (Fig. 13). The NaCN Raman first harmonic splitting into three components located at 2090.4, 2092, and 2097.8 cm^{-1} at 135 K (below T_{C2}), as it can be seen in Fig. 12, can be also fitted using Eqs. (35)–(37), assuming that these energy positions are related to $\nu_1(E^{\uparrow})$, $\nu_1(\bar{E})$, and $\nu_1(E\downarrow)$, respectively.

We observe that the Raman first harmonic splitting $\Delta(h\nu_1(E^{\uparrow\downarrow}))=-7.4\ \text{cm}^{-1}$ is in agreement with the ir second harmonic splitting $\Delta(h\nu_2(E^{\uparrow\downarrow}))=-15.7\ \text{cm}^{-1}$ obtained at 10 K with a larger electric field, and that the mean electric field at 135 K calculated from Eqs. (36) and (37) ($E=2.3\times10^7$ V/cm) has not yet reached its final low-temperature value of 2.47×10^7 V/cm.

For the KCN host lattice, where CN^- antiferroelectric ordering is also recognized, the first harmonic Raman splitting between $h\nu_1(E^{\uparrow})$ and $h\nu_1(E^{\downarrow})$ should be of the order of 4.5 cm^{-1} which is too small to make us able to differentiate the three components, but their existence is explained quite well by the unsymmetrical observed shape of the Raman mode below T_{C2}.

In summary, we recognize that the essential experimental facts observed below T_{C2} in NaCN and KCN, both for Raman and ir responses of the stretching harmonic position and shift under buildup of a mean electric field are quite well represented by the model given here.

RbCN and CsCN do not show any of the low-temperature phase transition manifestations as observed in KCN and NaCN. They show neither a shift to low energies of the ir second harmonic at a possible transition temperature of electric ordering, nor the appearance of oppositely shifting satellite absorption $\nu(E^{\uparrow})$. We can conclude, that no electric ordering appears at low temperature in these two cyanides.

D. Bandwidth of Raman and ir transitions

Let us finally discuss the bandwidth evolution under cooling as typically represented in Figs. 5 and 9. Mainly we have to explain the following.

The observed different ir and Raman bandwidth evolution in the high-temperature phase and at the order-disorder phase transition.

The broadening mechanism of the stretching in the intermediate phase of NaCN and KCN.

(a) In the high-temperature range where the structure is pseudocubic, the CN^- molecule can be regarded as a quasifree rotor. Infrared or Raman induced transitions connect rotating states of different vibrational levels of proper symmetry with selection rules $\Delta J=\pm1$ for ir and $\Delta J=0$ for Raman, where J is the rotational quantum number. Population distribution of rotational J states is temperature dependent and since rotational energy levels are not equally separated in a vibrational state, ir stretching transition width broadened by rotational motion is temperature dependent, while the Raman transition is unbroadened and quite temperature independent. At the order-disorder phase transition Raman bandwidth broadening ($\lesssim1\ \text{cm}^{-1}$ for the first harmonic Fig. 5) could be attributed to E_g and T_{2g} distortions of the lattice while for ir bandwidth, the narrowing occurs because of the abrupt decrease of rotational motion freedom in the ordered phase.

(b) In the intermediate phase of NaCN and KCN, we observe both in Raman and ir a bandwidth broadening under cooling. It is recognized that in this phase the CN^- molecule can reorient among two potential minima represented by the heat and tail exchange through excited positions. Under cooling in this structural phase, a local electric field, produced mainly by cationic displacement that leads to the low-temperature cationic distortion and responsible of the antiferroelectric order at low temperature, starts to build up. The CN^- molecule, in its motion, "feels" this electric field and the line shape represents directly the local electric field distribution seen by the molecule during its head and tail flip. This distribution broadens evenly around a zero mean value as the electric field strength increases, and contributes to the inhomogeneous broadening of the ir and Raman bands. In Fig. 13 the ir second harmonic peak position is presented together with its bandwidth (represented by arrows in the intermediate phase). It is interesting to notice that the arrows occupy the entire region of the low-temperature main and satellite energy positions. Below T_{C2} the slowing down process of CN^- rotation makes the electric field strength stronger and its distribution, as seen by the molecule, sharper. This allows the observation of the main properly aligned CN^- stretching transition and its $\nu(E^{\downarrow})$ satellite.

None of the above-mentioned phenomena are observed for RbCN and CsCN confirming that a mean static electric field is too small (if it exists) at low temperature in these materials.

IV. CONCLUSIONS

Our data, obtained by the Raman and ir response of the first, second, and third harmonics of CN^- stretching motion in a regular sublattice of CN^- ions in pure alkali cyanides, were used to construct a detailed anharmonic oscillator model, which however was simplified and restricted to individual CN^- ions. This seems justified, because dynamic coupling effects in the stretching motion of the closely and regularly spaced CN^- ions—which could in principle produce in-phase (Raman-active) and out-of-phase (ir-active) stretching modes of slightly different frequency in the antiferroelectric phase—are too weak to be detectable. On the other hand, the elastic and electric effects of the CN^- molecule surrounding influences in well measurable way the frequency position, width, spectral shape and strength of its anharmonic-

oscillator response. This allows us to determine by spectral measurements changes in volume, elastic deformations, CN^- rotational freedom, and mean electric fields from possible electric ordering throughout the temperature variation and the various phase transitions. Though oversimplified in some aspects, this anharmonic model developed for pure alkali cyanides of well-known structural behavior and transitions, will play an important role to study and clarify with the same spectral technique the electric and elastic order and disorder behavior of various dipole-diluted and mixed alkali cyanides, which are much less well established.[36]

ACKNOWLEDGMENTS

This work was supported by National Science Foundation (NSF) Grants Nos. DMR-81-05532 and DMR-87-06416. All reported experiments were performed at the University of Utah, while the first two authors were scientific visitors at University of Utah.

[1]H. Suga, T. Matsuo, and S. Seki, Bull. Chem. Soc. Jpn. **38**, 1115 (1965).
[2]J. M. Bijvoet and J. A. Lely, Rec. Trav. Chim. **59**, 908 (1940).
[3]J. A. Lely, Dissertation Utrecht, 1942; *Structure Reports 1942–1944,* edited by A. J. C. Wilson (NVA Oosterhock's Uitgevers, M.I.J., Utrecht), Vol. 9.
[4]G. S. Parry, Acta. Crystallogr. **15**, 601 (1962).
[5]J. M. Rowe, J. J. Rush, and F. Luty, Phys. Rev. B **29**, 2168 (1984).
[6]J. M. Rowe (private communication); G. Knopp, K. Knorr, and A. Loidl, Z. Phys. B **51**, 259 (1983).
[7]A. Cimino and G. S. Parry, Nuovo Cimento **19**, 971 (1961).
[8]P. Gash and F. Luty, J. Microsc. **140**, 351 (1985).
[9]M. D. Julian and F. Luty, Phys. Rev. B **21**, 1647 (1980).
[10]M. D. Julian and F. Luty, Ferroelectrics **16**, 201 (1977).
[11]F. Luty and J. Ortiz-Lopez, Phys. Rev. Lett. **50**, 1289 (1983).
[12]J. M. Rowe, J. J. Rush, N. Vagelatos, D. L. Price, D. G. Hinks, and S. Susman, J. Chem. Phys. **62**, 4551 (1975); J. M. Rowe, J. J. Rush, and E. Prince, *ibid.* **66**, 5147 (1977).
[13]D. Fontaine, These de Doctorat, Universite Paris VI, 1978 (unpublished).
[14]M. Sugisaki, T. Matsuo, H. Suga, and S. Seki, Bull. Chem. Soc. Jpn. **41**, 1747 (1968).
[15]T. Shimada, T. Matsuo, H. Suga, and F. Luty, J. Chem. Phys. **85**, 3530 (1986).
[16]K. H. Michel and J. Naudts, J. Chem. Phys. **67**, 547 (1977); **68**, 216 (1978).
[17]W. Dultz, J. Chem. Phys. **65**, 2812 (1976).
[18]D. Fontaine and H. Poulet, Phys. Status Solidi B **58**, 9 (1973).
[19]D. Durand, L. C. Scavarda do Carmo, A. Anderson, and F. Luty, Phys. Rev. B **22**, 4005 (1980).
[20]L. C. Scavarda do Carmo and F. Luty, Phys. Status Solidi B **89**, 149 (1978).
[21]A. Anderson, P. Gash, and F. Luty, Phys. Status Solidi B **105**, 315 (1981).
[22]L. Winchester, Ph.D. thesis, University of Illinois, 1975 (unpublished).
[23]W. D. Seward and V. Narayanamurti, Phys. Rev. **148**, 463 (1966).
[24]G. P. Field and W. F. Sherman, J. Chem. Phys. **47**, 2378 (1967).
[25]D. Durand and F. Luty, Ferroelectrics **16**, 205 (1977).
[26]L. C. Scavarda do Carmo, F. Luty, T. Holstein, and R. Orbach, Phys. Rev. B **23**, 3186 (1981).
[27]H. Ivey, Phys. Rev. **72**, 341 (1947).
[28]G. Herzberg, *Spectra of Diatomic Molecules* (Van Nostrand, New York, 1950).
[29]E. Fues, Ann. Phys. (Leipzig) **80**, 367 (1926).
[30]E. C. Kemble, J. Opt. Soc. Am. **12**, 1 (1926).
[31]J. L. Dunham, Phys. Rev. **35**, 1347 (1930).
[32]J. E. Gready, J. B. Bacskay, and N. S. Hush, Chem. Phys. **24**, 333 (1977).
[33]J. E. Gready, J. B. Bacskay, and N. S. Hush, Chem. Phys. **31**, 467 (1978).
[34]B. Koiller, M. A. Davidovich, L. C. Scavarda do Carmo, and F. Luty, Phys. Rev. B **29**, 3586 (1984).
[35]T. K. Ha and G. Zumofen, Mol. Phys. **40**, 445 (1980).
[36]D. Durand and F. Luty (unpublished).